NANO LETTERS

Letter

pubs.acs.org/NanoLett

Enzyme-Powered Hollow Mesoporous Janus Nanomotors

Xing Ma,[†] Anita Jannasch,[‡] Urban-Raphael Albrecht,[‡] Kersten Hahn,[§] Albert Miguel-López,[†] Erik Schäffer,[‡] and Samuel Sánchez*[,†,⊥,¶]

[†]Max Planck Institute for Intelligent Systems Institution, Heisenbergstraße 3, 70569 Stuttgart, Germany

[‡]Center for Plant Molecular Biology, University of Tübingen, Auf der Morgenstelle 32, 72076 Tübingen, Germany

[§]Stuttgart Center for Electron Microscopy, Max Planck Institute for Solid State Research, Heisenbergstraße 1, 70569 Stuttgart, Germany

[⊥]Institució Catalana de Recerca i Estudis Avancats (ICREA), Pg. Lluís Companys 23, 08010 Barcelona, Spain

[¶]Institut de Bioenginyeria de Catalunya (IBEC), Baldiri i Reixac 10-12, 08028 Barcelona, Spain

Supporting Information

ABSTRACT: The development of synthetic nanomotors for technological applications in particular for life science and nanomedicine is a key focus of current basic research. However, it has been challenging to make active nanosystems based on biocompatible materials consuming nontoxic fuels for providing self-propulsion. Here, we fabricate self-propelled Janus nanomotors based on hollow mesoporous silica nanoparticles (HMSNPs), which are powered by biocatalytic reactions of three different enzymes: catalase, urease, and glucose oxidase (GOx). The active motion is characterized by a mean-square displacement (MSD) analysis of optical video recordings and confirmed by dynamic light scattering (DLS) measurements. We found that the apparent diffusion coefficient was enhanced by up to 83%. In addition, using optical tweezers, we directly measured a holding force of 64 ± 16 fN, which was necessary to counteract the effective self-propulsion force generated by a single nanomotor. The successful demonstration of biocompatible enzyme-powered active nanomotors using biologically benign fuels has a great potential for future biomedical applications.

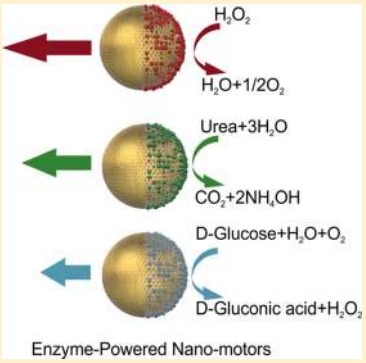

KEYWORDS: *Hollow mesoporous silica nanoparticles, nanomotors, enzyme, hybrid motors, Janus particles, optical tweezers*

Fabrication of chemically powered nanomotors capable of both autonomous motion and cargo delivery at small scales may lead to novel, active nanocarriers with potential biomedical relevance.[1−6] Ideally, the architecture of such nanomotors should be constructed by biocompatible and biodegradable materials enabling different propulsion pathways, that is, different catalysts conjugations that operate with biologically benign fuels. To meet such requirements, mesoporous silica of the MCM-41 (Mobil Composition of Matter No. 41)[7] type stands out as an ideal candidate for the nanomotor's body. Previous research indicated that mesoporous silica materials of spherical shape were nontoxic for cells and tissues within a certain concentration range up to 100 μg/mL and a size range from 80−500 nm.[8−10] The mesoporous structure of MCM-41 particles is advantageous for drug delivery in nanomedicine.[9−11] In particular, hollow mesoporous silica nanoparticles (HMSNPs) have been reported as a novel theranostic platform in the biomedical field because of their high drug-loading capacity given by the hollow structure and superior biocompatibility both *in vitro* and *in vivo*.[12,13] A new propulsion strategy replacing the common Pt/H_2O_2 combination to provide mechanical power for micro/nanomotors has been a long-standing goal in the community, but successful cases are rare. Although researchers presented motors consuming new fuels, for example, H_2 bubble propulsion by a metallic (Zn, Al, or Mg) reaction with acid[14] or H_2O,[15,16] the short lifetime and harsh reaction conditions limited their real applications. Biocatalytic reactions triggered by enzymes are rather promising because of their high reaction rate and variable choices of enzyme/fuel combinations.[17] Recent research has demonstrated that enzymes by themselves can act as self-propelled nanomotors,[18−20] in addition to being anchored to artificial "large" micro-objects (i.e., carbon nanotubes,[21] carbon fibers,[22] and microtubes[23,24]), to provide the propulsion force using catalytic reactions. Enzymatic reactions bring new insight into the possibility of using nontoxic fuel to drive motors. Therefore, the integration of HMSNPs and enzymes leads to a novel type of enzyme-powered nanomotors, which might be able to further achieve multiple functions within a biological environment. Because of the hollow structure and small dimensions, these biocompatible, enzymatic nanomotors might serve as active drug delivery nanosystems in future biomedical applications.

Here, we report the fabrication of Janus nanomotors based on HMSNPs using various enzymatic reactions for self-

Received: August 5, 2015
Revised: September 19, 2015
Published: October 5, 2015

DOI: 10.1021/acs.nanolett.5b03100
Nano Lett. 2015, 15, 7043−7050

Scheme 1. Fabrication of Enzymatic Hollow Mesoporous Silica Janus Nanomotors. (a) Synthesis of HMSNP by Using Solid SiO_2 Nanoparticles as Template, and Further Surface Modification of Amino Groups by Grafting Method To Produce HMSNP-NH_2; (b) Fabrication of JHMSNP-NH_2@SiO_2 by Electron Beam (e-beam) Evaporation of SiO_2 (10 nm) on a Monolayer of HMSNP-NH_2 and (c) Detachment of the Janus Nanoparticles by Sonication Treatment; (d) Conjugation of Enzymes onto One Face of the Janus Nanoparticles via a Glutaraldehyde (GA) Linker Molecule

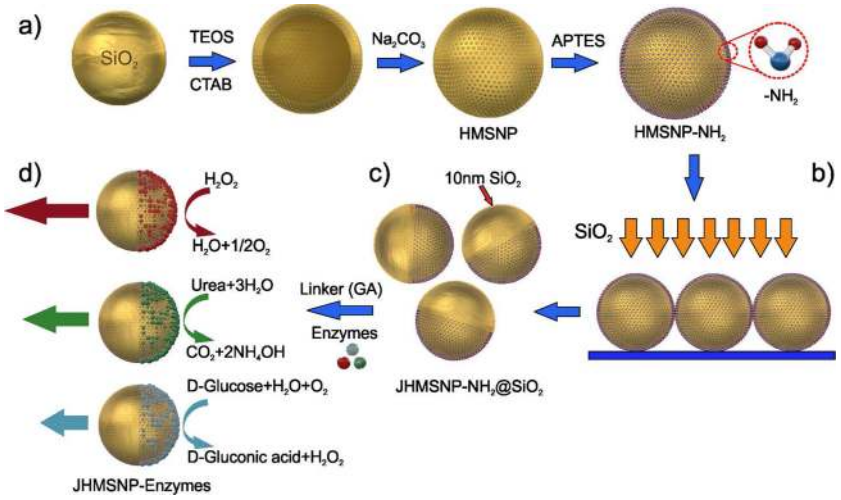

propulsion, as illustrated in Scheme 1. The Janus nanomotors are driven by a chemo-phoretic mechanism generated by these biocatalytic reactions happening asymmetrically at only one face of the Janus nanoparticles.[25−27] Given that the nanomotors are solely made of silica and enzymes, we expect the enzymatic nanomotors to possess good biocompatibility. To the best of our knowledge, this is the first demonstration of fully biocompatible Janus nanomotors using different biologically benign fuels, which are built up by nonmetallic components. Furthermore, the hollow spheres—composed of a mesoporous shell with nanochannels (2−3 nm) connecting the in- and outside—can serve as nanocontainers for drug delivery. Compared to previous passive drug delivery nanosystems, such self-propelled nanomotors might be able to actively transport drug molecules to targeted sites using methods such as chemotaxis,[28−30] pH taxis,[31] or remote magnetic guidance.[32,33]

The HMSNPs were synthesized by a selective etching method with minor modifications (Scheme 1a).[34,35] As a template, solid silica nanoparticles were first prepared by the Stöber method[36] and further coated with a mesoporous silica shell in an aqueous solution containing cetyltrimethylammonoium bromide (CTAB) and triethanolamine (TEOA). The solid silica core was removed by Na_2CO_3 in an aqueous solution, yielding HMSNPs. The hollow nanoparticles were further modified with amine groups (−NH_2) in an ethanol solution containing 3-aminopropyltriethoxysilane (APTES), denoted as HMSNP-NH_2. By dropping an ethanol solution containing HMSNP-NH_2 (5 mg/mL) onto a glass slide pretreated with an O_2 plasma, we prepared a monolayer of HMNSP-NH_2 on a glass slide and achieved an asymmetric nanoarchitecture by half-capping the hollow nanoparticles with a silicon dioxide (10 nm SiO_2) layer using electron beam (e-beam) deposition (Scheme 1b,c). The enzymes were covalently conjugated onto the noncoated side of the Janus nanoparticles via a glutaraldehyde (GA) linker molecule (Scheme 1d).[37,38] Each enzyme can then decompose the corresponding fuel and provide self-propulsion for the nanomotors as illustrated in Scheme 1, panel d.

The HMSNPs were characterized by transmission electron microscopy (TEM) (Figure 1a). The diameter of the hollow

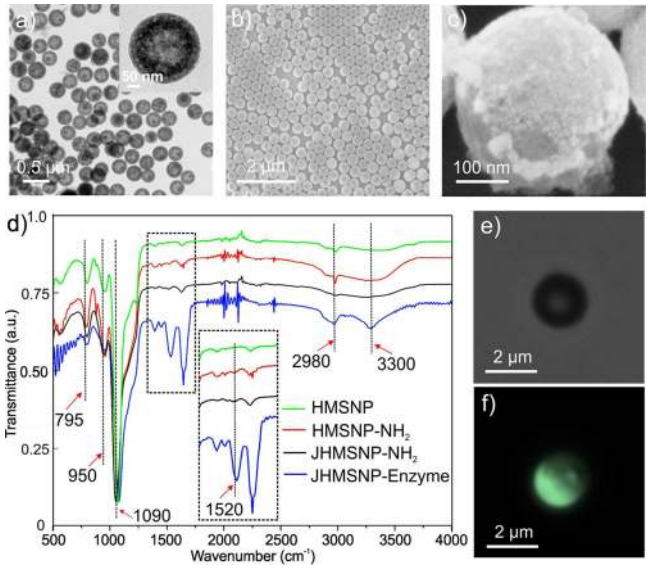

Figure 1. Fabrication and characterization of JHMSNP-enzyme as biocatalytic nanomotors. (a) TEM images of HMSNPs (inset is an enlarged image of a single HMSNP); (b) SEM image of a HMSNP-NH_2 monolayer prepared on a silicon wafer; (c) SEM image of an enzyme-coated JHMSNP (catalase). Note: the particle was half-coated with nickel for better contrast and observation of the Janus structure in panel c; (d) FTIR spectra of hollow nanoparticles with varied surface functional groups as indicated; (e) bright field and (f) fluorescence (FITC channel) images of FITC functionalized Janus SiO_2, 2-μm-diameter microparticles.

nanoparticles was estimated by measuring the size of 50 nanoparticles by ImageJ, and the value was found to be 389 ± 6 nm (average size ± standard error of mean, N = 50). The bright core of the nanoparticles in the TEM image (inset of Figure 1a) indicates their hollow structure. In Figure 1, panel b, a scanning electron microscopy (SEM) image of a monolayer of HMSNP-

DOI: 10.1021/acs.nanolett.5b03100
Nano Lett. 2015, 15, 7043−7050

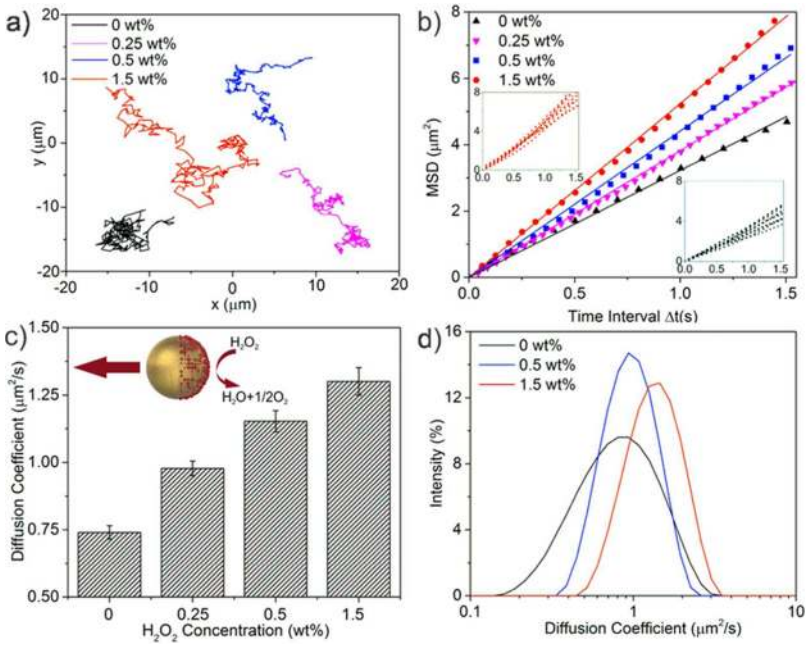

Figure 2. Analysis on the dynamic properties of the JHMSNP-Catalase nanomotors, (a) representative tracking trajectories of the nanomotor during 30 s. (b) Average MSD versus time interval (Δt) analyzed from tracking trajectories (insets are MSD curves of individual nanomotors at 0 and 1.5 wt % H_2O_2). (c) Diffusion coefficient values determined from the slope of the linear fitting curves of average MSD plots (for panels a–c, 30 nanoparticles were analyzed, and the error bars in panel c represent the standard error of mean, $N = 30$) and (d) diffusion coefficient histogram of the nanomotors measured by dynamic light scattering (DLS).

NH_2 is shown. Because of the monodispersity, we neither observed an overlap nor aggregation of the hollow nanoparticles, which is crucial for the subsequent Janus-structure fabrication. Through e-beam evaporation of SiO_2 with a thickness of 10 nm, we obtained hollow Janus nanoparticles, denoted as JHMSNP-NH_2@SiO_2. Then, we covalently attached, as a first enzyme, catalase to the noncoated side of the Janus nanoparticles by using GA as a linker molecule, which reacted with amine groups on both the Janus nanoparticle and the enzyme.[37,38] To better visualize the Janus structure under SEM in a control experiment, we replaced the deposited SiO_2 layer with a metallic element (e.g., nickel, Figure 1c).

The surface modification process was monitored by Fourier transform infrared spectroscopy (FTIR) spectra measurements (Figure 1d). Sharp peaks centered at 795 and 1090 cm^{-1} due to symmetric and asymmetric vibrations of Si–O, respectively, and a peak at 950 cm^{-1} assigned to the asymmetric vibration of Si–OH suggest that the base material of the nanomotors is composed of silica. Furthermore, the peaks at 2930 and 2980 cm^{-1} from $-CH_3$ and $-CH_2$, respectively, can be explained by the silica precursor, the TEOS molecule. After functionalization of the HMSNPs by a grafting method, a peak at 1520 cm^{-1} due to the N–H bond in the primary amines was found in HMSNP-NH_2. After the e-beam deposition, the peak of the primary amine (at 1520 cm^{-1}) remained, suggesting the survival of the surface functional groups during the e-beam deposition process. Upon enzyme conjugation to the hollow nanoparticles, the peak intensity of the amine group at 1520 cm^{-1} and of the $-CH_2$ groups at 2980 cm^{-1} significantly increased relative to the peak intensity of silica (795, 950, and 1090 cm^{-1}). We attribute this increase to the linkage of the enzymes containing a large quantity of amine groups. In addition to the FTIR spectra, zeta-potential measurements are also consistent with the surface functionalization process (Figure S1 and Table S2 in the Supporting Information). After the amine group modification, the negative surface charge of bare silica HMSNP of −36 ± 7 mV (average ± standard deviation (SD), $N = 10$) was reverted to a positive value of +31 ± 5 mV (average ± SD, $N = 10$). The half-sided coating of SiO_2 led to a surface charge decrease to +12 ± 5 mV (average ± SD, $N = 10$). This reduction is consistent with half of the amine groups being embedded under the SiO_2-coated layer and only amine groups at the noncoated side of the Janus nanoparticles being exposed and protonated. The enzyme attachment resulted in varied zeta-potential values, which depended on the enzyme and their different isoelectric points (Table S2 in the Supporting Information). For instance, the JHMSNP-catalase had the lowest surface charge value of −30 ± 5 mV (average ± SD, $N = 10$) compared to urease- and GOx-conjugated nanoparticles. The surface-charge difference of the three enzyme-conjugated Janus nanoparticles supports that the enzymes were conjugated to the surface of hollow Janus nanoparticles. Furthermore, we measured the enzymatic activity of the JHMSNP-enzyme conjugates, which further confirmed the presence of enzymes on the surface of the nanomotors (Figure S2 in the Supporting Information).

To further support the feasibility and better illustrate the fabrication strategy of the Janus nanomotors, we treated large, solid silica microspheres with a diameter of 2 μm with a similar process to produce Janus microparticles. We suspended these particles in an ethanol solution containing fluorescein isothiocyanate (FITC) (1 mg/mL), a florescence dye containing an isothiocyanate reactive group (–N=C=S) group that is ready to react with amine groups on the noncoated side of the Janus SiO_2 microparticles. After an extensive wash with ethanol to remove unconjugated FITC, the green fluorescence color was only observed on a hemisphere of the microspheres (Figure 1e,f), indicating the feasibility of

DOI: 10.1021/acs.nanolett.5b03100
Nano Lett. 2015, 15, 7043–7050

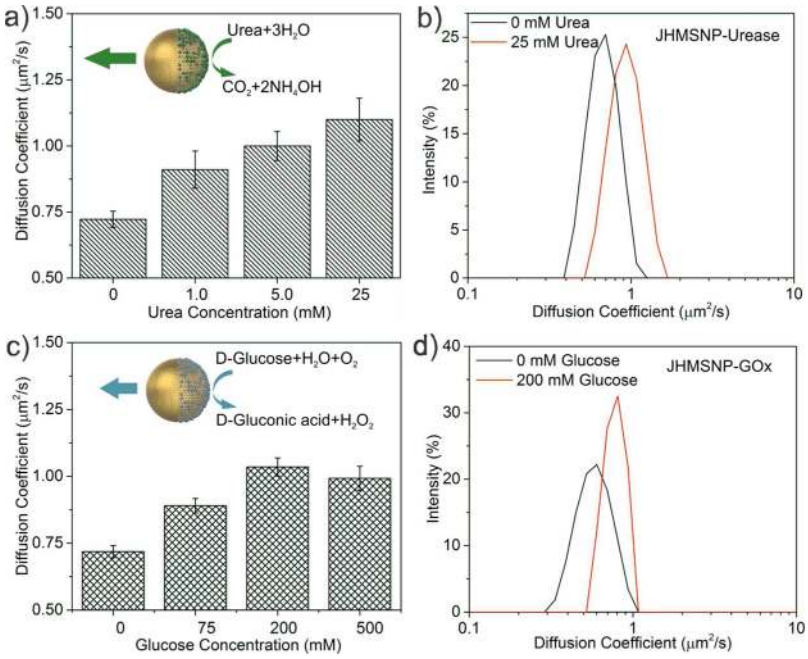

Figure 3. Enhanced diffusion of the (a, b) JHMSNP-urease and (c, d) JHMSNP-GOx nanomotors. Panels a and c are the diffusion coefficients of the two nanomotors determined from MSD analysis; panels b and d are diffusion coefficient histograms measured by DLS. (For panels a and c, and the error bars represent the standard error of mean, $N = 30$.)

covalently conjugating molecules onto the noncoated side of the Janus particles via a chemical reaction with the amine groups.

Active motion of the self-propelled enzymatic nanomotors is driven by the gradient of the chemical species produced by asymmetric biocatalytic reactions that only take place at one face of the Janus nanomotors.[25−27] The self-propelled motion of the nanomotors was systematically investigated by a mean-square-displacement (MSD) analysis (see detailed methods in the Supporting Information). The time-dependent tracking process of JHMSNP-catalase with and without H_2O_2 fuel up to 25 s is given as an example in Figure S3 in the Supporting Information. Typical tracking trajectories of the nanomotors in the presence of the corresponding fuel, that is, H_2O_2 for JHMSNP-catalase, are presented in Figure 2, panel a. Because of the small diameter of less than 400 nm, the nanomotors have a very high rotational diffusion coefficient D_r, which is proportional to $1/r^3$ given by the equation $D_r = k_BT/(8\pi\eta r^3)$, where k_B is the Boltzmann constant, T the absolute temperature, η the viscosity of the solution, and r the radius of the nanoparticles. In our case, the time interval Δt between frames ($\approx$ 0.05 s or about 20 frames per second) was comparable to the rotational time $\tau \approx D_r^{-1} \approx 0.07$ s. For times longer than τ, the value of the long-time translational diffusion coefficient D_L can be extracted from the slope of MSD plots both in the presence and absence of fuel by the equation, MSD $= 4D_L\Delta t$.[39−41] In the absence of fuel, the long-time diffusion coefficient is equal to the translational diffusion coefficient $D_t = k_BT/(6\pi\eta r)$ according to the Stokes−Einstein equation (no fuel: $D_L = D_t$).

We expected that the self-propelled nanomotors would exhibit enhanced diffusion for times longer than the rotational diffusion time of the nanomotors as discussed earlier. Indeed, we observed an increased slope of the average MSD versus Δt (Figure 2b). The enzymatic Janus nanomotors showed a fuel-concentration-dependent enhanced diffusion (Figure 2b,c). During the time range under study, the apparent long-time translational diffusion coefficient of JHMSNP-catalase was found to be 1.30 ± 0.05 $\mu m^2/s$, which increased by about 83% at 1.5 wt % H_2O_2 compared to the value of 0.75 ± 0.03 $\mu m^2/s$ without fuel. Independently, the active motion of the self-propelled Janus nanomotors was further investigated by another technique, dynamic light scattering (DLS) (Figure 2d). DLS takes advantage of the size-dependent Brownian motion to characterize the nanoparticles' size by measuring their inherent diffusion coefficient based on the Stokes−Einstein equation. In our study, we used DLS to measure the diffusion coefficient of the nanomotors in solution. The histogram of the diffusion coefficient right-shifted to higher values when the nanomotors were fueled (from the black curve to blue and red ones, Figure 2d). From the DLS measurements, the average diffusion coefficient of the nanomotors without fuel was 0.67 $\mu m^2/s$ (polydispersity index (PDI) = 0.244), which was enhanced by 85% to a value of 1.24 $\mu m^2/s$ (PDI = 0.384) at 1.5 wt % H_2O_2. The DLS results agree very well with the MSD analysis, and both methods show that the self-propulsion of the nanomotors is driven by the biocatalytic chemical reactions.

Since H_2O_2 is not biocompatible, we coupled two more enzymes, urease and GOx, to the Janus hollow nanoparticles, which are powered by the biocompatible fuels of urea and glucose, respectively. These fuels are naturally present in a biological environment; for example, the average concentration of urea and glucose in human blood is about 5−10 mM.[42,43] Typical tracking trajectories and MSD plots of the two nanomotors are presented in Figure S4 in the Supporting Information. Upon addition of the corresponding fuels, the apparent diffusion coefficient of the two nanomotors increased by 52% and 38%, at 25 mM urea and 500 mM glucose, respectively (Figure 3a,c). We also used DLS to measure the enhanced diffusion. As with the catalase nanomotors, the DLS measurements showed a right-shift of the diffusion coefficient histogram when urea and glucose were added (Figure 3b,d).

DOI: 10.1021/acs.nanolett.5b03100
Nano Lett. 2015, 15, 7043−7050

Table 1. Apparent Diffusion Coefficient Determined from the MSD Analysis. (Average ± Standard Error of Mean, N = 30)

H_2O_2	JHMSNP-catalase	urea	JHMSNP-urease	glucose	JHMSNP-GOx
0 wt %	0.75 ± 0.03 $\mu m^2/s$	0 mM	0.72 ± 0.03 $\mu m^2/s$	0 mM	0.72 ± 0.02 $\mu m^2/s$
0.25 wt %	0.98 ± 0.03 $\mu m^2/s$	1 mM	0.91 ± 0.04 $\mu m^2/s$	75 mM	0.89 ± 0.03 $\mu m^2/s$
0.5 wt %	1.15 ± 0.04 $\mu m^2/s$	5 mM	1.01 ± 0.06 $\mu m^2/s$	200 mM	1.04 ± 0.03 $\mu m^2/s$
1.5 wt %	1.30 ± 0.05 $\mu m^2/s$	25 mM	1.10 ± 0.08 $\mu m^2/s$	500 mM	0.99 ± 0.05 $\mu m^2/s$

With a fuel concentration higher than 200 mM, the enhancement of apparent diffusion for JHMSNP-GOx saturated. We attribute the saturation to two effects. First, the Michaelis−Menten enzyme kinetics of GOx, having a K_m value of about 33−110 mM,[44,45] implies that the catalytic reaction rate should be saturated at 500 mM glucose. Second, the viscosity of the glucose solution is higher compared to that of pure water. For the 500 mM glucose solution, the viscosity increased by about 13% at 22 °C[46] at which temperature we carried out the experiments. The viscosity increase counteracts the enhancement of the diffusion coefficient according to the Stokes−Einstein equation.

The results of the diffusion coefficient for the three nanomotors determined from the MSD analysis are summarized in Table 1. For all three Janus nanomotors' Brownian motion, the measured value of D_t was about 0.72−0.75 $\mu m^2/s$, which is slightly lower than the theoretical value of 1.07 $\mu m^2/s$, assuming a diameter of 400 nm for the nanoparticle at room temperature of 22 °C. We attribute the lower value to a size increase after the e-beam deposition (10 nm) and the conjugation of the nanometer-sized enzymes (10−30 nm). Also, the hydrodynamic size is inherently larger than the real particle size. In addition, larger, slower moving particles had a higher contrast in the video images and were less affected by motion blur in the video images. Therefore, the selection of the traced particles may have been biased toward larger particles. The three enzymatic nanomotors had a different efficiency of self-propulsion upon fuel addition, which might be explained by the different enzymatic activity of the three enzymes.[47−49] We confirmed the catalytic activity of the nanomotors by measuring the concentration of the reaction products (Figure S2 in the Supporting Information). The three nanomotors had different enzymatic activities: 3.29 μmol O_2, 7.94 × 10^{-2} μmol NH_3, 3.42 × 10^{-4} μmol H_2O_2 per μg HMSNP min, for the catalase-, urease-, and GOx-coupled nanomotors, respectively. The catalase-based nanomotor showed the highest reaction rate, which was also reflected in the estimated catalytic activity per particle (see caption of Figure S2 in the Supporting Information). We also found a stable biocatalytic rate during the initial period, when the fuel concentration and enzyme activity was approximately constant. With increasing time, the enzymatic reaction rate decreased, possibly due to fuel depletion. To avoid artifacts and a possible decrease in enzymatic activity, we recorded all videos within the initial 3−5 min. Consistent with the MSD measurements, the diffusion coefficient distribution of the JHMSNP-catalase nanomotor based on DLS measurements right-shifted the most (Figure 2d), while that of GOx right-shifted least (Figure 3d). We further evaluated the cytotoxicity of the enzymatic nanomotors and the corresponding fuels by a MTT (3-(4,5-dimethylthiazol-2-yl)-2,5-diphenyltetrazolium bromide) assay (Figure S5 in the Supporting Information). Although JHMSNP-catalase had low cytotoxicity (Figure S5a in the Supporting Information), H_2O_2 showed a toxic effect at a extremely low concentration of 4 × 10^{-3} wt % (Figure S5b in the Supporting Information). This toxicity excludes catalase-based motors for applications in a physiological environment. The fuels of urease and glucose demonstrate no toxic effect toward HeLa cells within the concentration range we studied (1−100 mM) (Figure S5d,f in the Supporting Information). Notably, JHMSNP-urease was biocompatible with a low toxicity effect—up to 80% cell viability at high concentration (32 μg/mL). Only the JHMSNP-GOx (Figure S5e in the Supporting Information) showed a slightly higher toxic effect than JHMSNP-catalase and JHMSNP-urease (Figure S5c in the Supporting Information), which we attribute to the production of toxic H_2O_2 produced by the conjugated GOx. Thus, the urease and GOx based nanomotors can be regarded as fully biocompatible considering the low cytotoxicity of the nanomotors and nontoxic effect of urea and glucose. In summary, we successfully fabricated enzyme-powered nanomotors that exhibit enhanced diffusion when fuel was added. The variable choice of enzyme/fuel combinations allowed us to achieve fully biocompatible micro/nanomotors driven by nontoxic fuels such as urea and glucose. Because these fuels are naturally present in a physiological environment, our enzyme-powered nanomotors may act as active drug delivery nanosystems given proper directionality guidance.

The self-propulsion implies that an effective force was acting on the nanomotors. How large is this force? On the basis of a theory for self-propelled particles, we can use the long-time translational diffusion coefficient to calculate the force.[39] For a spherical particle with two rotational degrees of freedom, the absolute value of the effective driving force is

$$F = \frac{3k_BT}{2r}\sqrt{2\left(\frac{D_L}{D_t} - 1\right)}$$

The concept of an effective, external self-propulsion force has been controversial, but recently it has been demonstrated to be a valid and useful concept.[50,51] By using the values for the JHMSNP-catalase at a 0.5 wt % hydrogen peroxide concentration (Table 1), the estimated driving force is F = 32 ± 8 fN.

To measure the effective driving force of the self-propelled Janus nanomotors directly, we used stable, high-resolution optical tweezers.[52,53] Optical tweezers act like a three-dimensional Hookean spring, where the force F is determined by the spring constant or trap stiffness κ and the displacement Δx of particle from the trap center ($F = \kappa\ \Delta x$). Since the average instantaneous thermal force that drives Brownian motion (~40 pN for our nanomotors[54]) is much larger than the holding force for the self-propelled particles, displacements due to the active effective driving force are not directly visible in the time traces $x(t)$ of a trapped nanomotor. Therefore, we measured the power spectral density (PSD) of the thermal motion for trapped nanomotors without fuel and with 0.5 wt % H_2O_2. The PSD describes how the variance of the data $x(t)$ is distributed over frequency space. By multiplying the particle displacements with the measured trap stiffness, we calculated

DOI: 10.1021/acs.nanolett.5b03100
Nano Lett. 2015, 15, 7043−7050

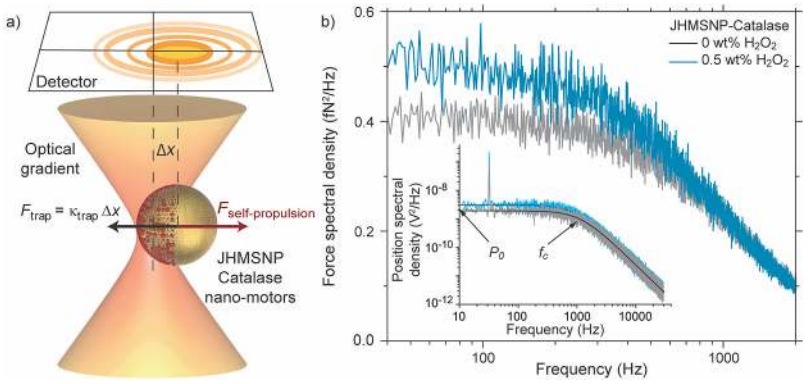

Figure 4. (a) Schematic illustration of the force measurement by optical tweezers. (b) Force spectral density as a function of frequency (lin-log plot) averaged over JHMSNP-catalase particles without (gray) and with fuel (cyan) (N = 15, N = 12 respectively). Inset: example PSD for a single JHMSNP-catalase particle without and with fuel averaged over 40 s. The spectrum features a calibration peak at 32 Hz (see Supporting Information). The dark lines are fits to the data.

the force spectral density. The difference in force spectral density for nanomotors with and without fuel, integrated over frequency space, is the net effective driving force of the nanomotors.

Power spectra of a single trapped nanomotor with and without fuel had a characteristic Lorentzian shape (inset of Figure 4b). From the Lorentzian, we determined the corner frequency $f_c = \kappa/(2\pi\gamma)$ and a zero-frequency plateau value $P_0 = D_L/(\pi f_c)^2$ proportional to the long-time diffusion coefficient $D_L = k_B T_{eff}/\gamma$, where γ is the drag coefficient, and T_{eff} is an effective temperature that accounts for the active motion (no fuel: $T_{eff} = T$, and $D_L = D_t$). We measured these parameters directly using our calibration technique.[55,56] To rule out variations due to particle size, we averaged the values of the individual parameters and the PSDs of many particles. There was no significant difference in the trap stiffness κ, the drag coefficient γ, and the displacement sensitivity β for all spatial directions for nanomotors with and without fuel (Table S1). Also, we confirmed that the voltage-to-force conversion factor $c = \kappa\beta$, which converts the recorded voltage signal from the optical tweezers photodiode detector to a force, was constant.[57] This parameter is based on the conservation of optical momentum and is independent of the size, shape, and material properties of the trapped particle. Thus, if we multiply our raw data with this factor and convert it to forces, we do not have to make any assumptions about the trapped object or the shape of the response curve in frequency space.

For nanomotors with fuel, we measured an increased force spectral density—a significant increase of the plateau value P_0 and, thus, an increase in the long-time diffusion coefficient D_L. The average force spectral density with fuel was larger at low frequencies compared to the one recorded in the absence of fuel (Figure 4b). The difference between the average force spectral densities with and without fuel resulted in an active effective driving force of $F = 64 \pm 16$ fN integral up to 1 kHz, error approximately based on the relative error of the P_0 difference:

$$\frac{\Delta F}{F} \approx \sqrt{\frac{(\Delta P_0^{\text{fuel}})^2 + (\Delta P_0^{\text{no fuel}})^2}{(P_0^{\text{fuel}} - P_0^{\text{no fuel}})^2}}$$

This directly measured value is consistent with the calculated value determined from the MSD measurements and confirms the activity of the enzyme-driven system. Also, the measurement in itself demonstrates that an effective, external self-propulsion force can be measured using optical tweezers for nanomotors.[50,51] Qualitatively, the force we measured is the absolute value of the average holding force necessary to stop the particle's motion if it would be solely moving in a single direction in the absence of Brownian motion. In terms of the theory, it is the absolute value of the effective "internal" force that is included in the Langevin equation.[32,43] This force is acting in a direction constantly changing due to the inherent rotational Brownian motion of the Janus particle. At present, we cannot deduce the force from the individual, molecular turnover events of the enzyme-driven, chemo-phoretic mechanism.

In summary, we successfully fabricated biocompatible enzyme-powered Janus nanomotors based on HMSNPs. The self-propelled Janus nanomotors were powered by biocatalytic reactions of three different enzyme/fuel combinations including catalase/H_2O_2, urease/urea, and GOx/glucose. The active motion of the Janus nanomotors was systematically characterized by a MSD analysis based on optical microscopy tracking of the nanomotors. The enhanced diffusion of the nanomotors was further confirmed by DLS measurements. For the first time, to the best of our knowledge, we measured the effective external force generated by a single nanomotor using optical tweezers. Moreover, we demonstrated fully biocompatible nanomotors driven by nontoxic fuels. Because the nanoparticles are small and hollow, the enzymatic Janus nanomotors investigated here are promising candidates for future biomedical applications. Following research efforts might be devoted to increasing the effective driving force and to guiding the biocompatible nanomotors by external manipulation methods, such as chemotaxis, pH taxis, thermos-taxis, magnetic control, or ultrasound, leading to directional movement of the nanomotors for active drug delivery into target locations.

■ ASSOCIATED CONTENT

Supporting Information

The Supporting Information is available free of charge on the ACS Publications website at DOI: 10.1021/acs.nanolett.5b03100.

Experimental sections about synthesis of hollow mesoporous Janus nanomotors, enzymatic activity assay, video recording and MSD analysis, power spectral density analysis, and toxicity evaluation of the nano-

DOI: 10.1021/acs.nanolett.5b03100
Nano Lett. 2015, 15, 7043−7050

motors and corresponding fuels; figures related to the zeta-potential measurements, enzymatic activity of nanomotors, and toxicity evaluation, and video snapshots of typical tracking of the nanomotors (PDF)

Typical videos of nanomotors without and with fuel (ZIP)

AUTHOR INFORMATION

Corresponding Author

*E-mail: sanchez@is.mpg.de; ssanchez@ibecbarcelona.eu.

Author Contributions

X.M. and S.S. initiated this project. X.M. prepared the enzymatic nanomotors and carried out experiments of SEM imaging, DLS measurement, optical video recording and MSD analysis, and enzymatic activity analysis. A.M.-L. developed the code for MSD analysis. K.H. conducted the TEM imaging. A.J., U.-R.A., and E.S. completed the optical trapping measurement. S.S. supervised the project. X.M., E.S., and S.S. analyzed the results and wrote the paper.

Notes

The authors declare no competing financial interest.

ACKNOWLEDGMENTS

The authors thank Prof. P. Fischer for instruments support. We also thank Alejandro Posada for the art design of the schematic figures. The research leading to these results has received funding from the European Union Seventh Framework Program [FP/2007/2013] under Grant Agreement No. 312483 (ESTEEM2), European Research Council under the European Union's Seventh Framework Program (FP7/20072013)/ERC Grant Agreement No. 311529 (LT-NRBS) and No. 260875 (Nanomech), the Eberhard Karls Universität Tübingen, and the Alexander von Humboldt Foundation.

REFERENCES

(1) Wang, H.; Pumera, M. *Chem. Rev.* **2015**, *115*, 8704−8735.
(2) Sánchez, S.; Soler, L.; Katuri, J. *Angew. Chem., Int. Ed.* **2015**, *54*, 1414−1444.
(3) Guix, M.; Mayorga-Martinez, C. C.; Merkoçi, A. *Chem. Rev.* **2014**, *114*, 6285−6322.
(4) Wang, J. *Nanomachines: Fundamentals and Applications*; Wiley-VCH: Weinheim, 2013.
(5) Duan, W.; Wang, W.; Das, S.; Yadav, V.; Mallouk, T. E.; Sen, A. *Annu. Rev. Anal. Chem.* **2015**, *8*, 311−333.
(6) Patra, D.; Sengupta, S.; Duan, W.; Zhang, H.; Pavlick, R.; Sen, A. *Nanoscale* **2013**, *5*, 1273−1283.
(7) Kresge, C. T.; Leonowicz, M. E.; Roth, W. J.; Vartuli, J. C.; Beck, J. S. *Nature* **1992**, *359*, 710−712.
(8) Asefa, T.; Tao, Z. *Chem. Res. Toxicol.* **2012**, *25*, 2265−2284.
(9) He, Q.; Shi, J. *J. Mater. Chem.* **2011**, *21*, 5845−5855.
(10) Slowing, I. I.; Vivero-Escoto, J. L.; Wu, C.-W.; Lin, V. S. Y. *Adv. Drug Delivery Rev.* **2008**, *60*, 1278−1288.
(11) Ambrogio, M. W.; Thomas, C. R.; Zhao, Y.-L.; Zink, J. I.; Stoddart, J. F. *Acc. Chem. Res.* **2011**, *44*, 903−913.
(12) Luo, Z.; Ding, X.; Hu, Y.; Wu, S.; Xiang, Y.; Zeng, Y.; Zhang, B.; Yan, H.; Zhang, H.; Zhu, L.; Liu, J.; Li, J.; Cai, K.; Zhao, Y. *ACS Nano* **2013**, *7*, 10271−10284.
(13) Ma, X.; Zhao, Y.; Ng, K. W.; Zhao, Y. *Chem. - Eur. J.* **2013**, *19*, 15593−15603.
(14) Gao, W.; Uygun, A.; Wang, J. *J. Am. Chem. Soc.* **2012**, *134*, 897−900.
(15) Gao, W.; Pei, A.; Wang, J. *ACS Nano* **2012**, *6*, 8432−8438.
(16) Li, J.; Singh, V. V.; Sattayasamitsathit, S.; Orozco, J.; Kaufmann, K.; Dong, R.; Gao, W.; Jurado-Sanchez, B.; Fedorak, Y.; Wang, J. *ACS Nano* **2014**, *8*, 11118−11125.
(17) Gao, J.; Ma, S.; Major, D. T.; Nam, K.; Pu, J.; Truhlar, D. G. *Chem. Rev.* **2006**, *106*, 3188−3209.
(18) Sengupta, S.; Dey, K. K.; Muddana, H. S.; Tabouillot, T.; Ibele, M. E.; Butler, P. J.; Sen, A. *J. Am. Chem. Soc.* **2013**, *135*, 1406−1414.
(19) Muddana, H. S.; Sengupta, S.; Mallouk, T. E.; Sen, A.; Butler, P. J. *J. Am. Chem. Soc.* **2010**, *132*, 2110−2111.
(20) Mikhailov, A. S.; Kapral, R. *Proc. Natl. Acad. Sci. U. S. A.* **2015**, *112*, E3639−E3644.
(21) Pantarotto, D.; Browne, W. R.; Feringa, B. L. *Chem. Commun.* **2008**, *10*, 1533−1535.
(22) Mano, N.; Heller, A. *J. Am. Chem. Soc.* **2005**, *127*, 11574−11575.
(23) Sanchez, S.; Solovev, A. A.; Mei, Y.; Schmidt, O. G. *J. Am. Chem. Soc.* **2010**, *132*, 13144−13145.
(24) Orozco, J.; García-Gradilla, V.; D'Agostino, M.; Gao, W.; Cortés, A.; Wang, J. *ACS Nano* **2013**, *7*, 818−824.
(25) Wang, W.; Duan, W. T.; Ahmed, S.; Mallouk, T. E.; Sen, A. *Nano Today* **2013**, *8*, 531−554.
(26) Golestanian, R.; Liverpool, T. B.; Ajdari, A. *Phys. Rev. Lett.* **2005**, *94*, 220801.
(27) Thakur, S.; Kapral, R. *J. Chem. Phys.* **2011**, *135*, 024509.
(28) Baraban, L.; Harazim, S. M.; Sanchez, S.; Schmidt, O. G. *Angew. Chem., Int. Ed.* **2013**, *52*, 5552−5556.
(29) Hong, Y.; Blackman, N. M. K.; Kopp, N. D.; Sen, A.; Velegol, D. *Phys. Rev. Lett.* **2007**, *99*, 178103.
(30) Dey, K. K.; Das, S.; Poyton, M. F.; Sengupta, S.; Butler, P. J.; Cremer, P. S.; Sen, A. *ACS Nano* **2014**, *8*, 11941−11949.
(31) Dey, K. K.; Bhandari, S.; Bandyopadhyay, D.; Basu, S.; Chattopadhyay, A. *Small* **2013**, *9*, 1916−1920.
(32) Baraban, L.; Makarov, D.; Streubel, R.; Monch, I.; Grimm, D.; Sanchez, S.; Schmidt, O. G. *ACS Nano* **2012**, *6*, 3383−3389.
(33) Khalil, I. S. M.; Magdanz, V.; Sanchez, S.; Schmidt, O. G.; Misra, S. *Int. J. Adv. Robot. Syst.* **2015**, *12*, 1−7.
(34) Chen, Y.; Chen, H.; Guo, L.; He, Q.; Chen, F.; Zhou, J.; Feng, J.; Shi, J. *ACS Nano* **2010**, *4*, 529−539.
(35) Fang, X.; Chen, C.; Liu, Z.; Liu, P.; Zheng, N. *Nanoscale* **2011**, *3*, 1632−1639.
(36) Stöber, W.; Fink, A.; Bohn, E. *J. Colloid Interface Sci.* **1968**, *26*, 62−69.
(37) Zhang, X.; Guan, R.-F.; Wu, D.-Q.; Chan, K.-Y. *J. Mol. Catal. B: Enzym.* **2005**, *33*, 43−50.
(38) Libertino, S.; Giannazzo, F.; Aiello, V.; Scandurra, A.; Sinatra, F.; Renis, M.; Fichera, M. *Langmuir* **2008**, *24*, 1965−1972.
(39) ten Hagen, B.; van Teeffelen, S.; Lowen, H. *J. Phys.: Condens. Matter* **2011**, *23*, 194119.
(40) Howse, J. R.; Jones, R. A.; Ryan, A. J.; Gough, T.; Vafabakhsh, R.; Golestanian, R. *Phys. Rev. Lett.* **2007**, *99*, 048102.
(41) Dunderdale, G.; Ebbens, S.; Fairclough, P.; Howse, J. *Langmuir* **2012**, *28*, 10997−11006.
(42) MacKay, E. M.; MacKay, L. L. *J. Clin. Invest.* **1927**, *4*, 295−306.
(43) Somogyi, M. *J. Biol. Chem.* **1945**, *160*, 69−73.
(44) Swoboda, B. E. P.; Massey, V. *J. Biol. Chem.* **1965**, *240*, 2209−2215.
(45) Gibson, Q. H.; Massey, V.; Swoboda, B. E. P. *J. Biol. Chem.* **1964**, *239* (11), 3927−3934.
(46) Telis, V. R. N.; Telis-Romero, J.; Mazzotti, H. B.; Gabas, A. L. *Int. J. Food Prop.* **2007**, *10*, 185−195.
(47) Tsuge, H.; Natsuaki, O.; Ohashi, K. *J. Biochem.* **1975**, *78*, 835−843.
(48) Karplus, P. A.; Pearson, M. A.; Hausinger, R. P. *Acc. Chem. Res.* **1997**, *30*, 330−337.
(49) Goldblith, S. A.; Proctor, B. E. *J. Biol. Chem.* **1950**, *187*, 705−709.
(50) ten Hagen, B.; Wittkowski, R.; Takagi, D.; Kümmel, F.; Bechinger, C.; Löwen, H. *J. Phys.: Condens. Matter* **2015**, *27*, 194110.

DOI: 10.1021/acs.nanolett.5b03100
Nano Lett. 2015, 15, 7043−7050

(51) Takatori, S. C.; Yan, W.; Brady, J. F. *Phys. Rev. Lett.* **2014**, *113*, 028103.
(52) Mahamdeh, M.; Pérez Campos, C.; Schäffer, E. *Opt. Express* **2011**, *19*, 11759−11768.
(53) Mahamdeh, M.; Schäffer, E. *Opt. Express* **2009**, *17*, 17190−17199.
(54) Taylor, E. *Nature* **2001**, *413*, 572−572.
(55) Tolić-Nørrelykke, S. F.; Schäffer, E.; Howard, J.; Pavone, F. S.; Jülicher, F.; Flyvbjerg, H. *Rev. Sci. Instrum.* **2006**, *77*, 103101.
(56) Schäffer, E.; Nørrelykke, S. F.; Howard, J. *Langmuir* **2007**, *23*, 3654−3665.
(57) Farré, A.; Marsà, F.; Montes-Usategui, M. *Opt. Express* **2012**, *20*, 12270−12291.

DOI: 10.1021/acs.nanolett.5b03100
Nano Lett. 2015, 15, 7043−7050